Chinese Journal of Chemical Engineering 25 (2017) 1273–1281

Contents lists available at ScienceDirect

Chinese Journal of Chemical Engineering

journal homepage: www.elsevier.com/locate/CJChE

Chemical Engineering Thermodynamics

A new model to predict the densities of nanofluids using statistical mechanics and artificial intelligent plus principal component analysis

F. Yousefi *, Z. Amoozandeh

Department of Chemistry, Yasouj University, Yasouj, 75914-353, Iran

ARTICLE INFO

Article history:
Received 17 February 2016
Received in revised form 23 October 2016
Accepted 24 October 2016
Available online 22 November 2016

Keywords:
Nanofluids
ANN
Equation of state
Model

ABSTRACT

In this work, some thermodynamic properties of nanofluids such as Sb_2O_5; SnO_2/(EG + H_2O), ZnO/(EG + H_2O), Al_2O_3/(EG + H_2O), ZnO/(PEG + H_2O), ZnO/PEG, and TiO_2/EG were estimated from the extended Tao–Mason equation of state, together with the Pak and Cho equation in various temperature, pressure, and volume fractions. The equations of state using minimum input data and density at room temperature as scaling constants, were developed to estimated densities of the above mentioned nanofluids. Furthermore, the artificial neural network plus principal component analysis (PCA) technique (with 20 neuron in hidden layer) was performed over the whole range of available conditions. The AADs of the calculated molar densities of all nanofluids using the EOS and ANN at various temperatures and volume fractions are 1.11% and 0.48%, respectively. In addition, the heat capacity and isentropic compressibility of the above mentioned nanofluids are predicted using obtained densities of EOS with the Pak and Cho equation.

1. Introduction

Nanofluids are two phase mixtures consisting of solid nanoparticles with sizes varying generally from 1 to 100 nm dispersed within heat transfer liquids such as water, ethylene glycol, propylene glycol, and light oils. Thermal properties and stability of nanofluids have been a hotly discussed topic during the last two decades due to their potential for application in heat transfer [1].

Nanofluids, firstly described by Choi [2] and other researchers, discover a new type of heat transfer fluid superior to conventional microparticle fluids in terms of thermophysical properties [2]. Moreover, enhancing heat transfer eliminates problems arising from microparticle fluids. Therefore, nanofluids have valuable applications in practical heat transfer processes due to their high potential for enhancement of heat transfer. The thermophysical properties of nanofluids, such as thermal conductivity, viscosity, and density, are important in heat transfer application involving heat transfer fluid for thermal engineering [3].

Among the various thermophysical properties of nanofluids, most attention has been dedicated to thermal conductivity and viscosity [4–8], while less attention has been paid to other properties such as density (ρ), specific heat capacity (C_p), and isentropic compressibility (K_s). Thermal conductivity and viscosity are not adequate to calculate theoretical heat transfer coefficient. Density, specific heat, and isentropic compressibility are also very significant for heat transfer computations. Therefore, these properties should perfectly determine because of their influence on nanofluid flow and heat transfer characteristics [9]. On the other hand, experimental evaluation of nanofluids suffers from limitations such as complexities in preparing monodisperse suspensions; and methodical problems in measuring particle size, concentration, and the homogeneity of its solution. As a consequence, the ranges of the considered variables are also limited. Hence a few density measurements have been presented for various nanofluids at different situations [10], while suggesting the reported theoretical correlation for the evaluation of nanofluids density is based on simple model.

Earlier, Ihm–Song–Mason equation of state (ISM EOS) [11] and Tao–Mason equation of state (TM EOS) [12] were extended to fluid and fluid mixtures [13–21]. In addition, the applications of equation of state and artificial neural networks approaches [19,22] were studied to approximate the properties of pure polymers. Generally, the artificial neural network (ANN) is a powerful and successful method for complex nonlinear systems due to unique advantages such as high speed, simplicity, and large capacity which reduce engineering attempt. In recent years, ANN modelling has been successfully used for predicting of thermophysical properties of pure and mixture fluids [22–26].

This research is focused on the capability of both TM EOS (with the Pak and Cho equation) and the ANN to estimate thermodynamic properties of nanofluids in different conditions. As a final point, the

* Corresponding author.
E-mail address: fyousefi@mail.yu.ac.ir (F. Yousefi).

http://dx.doi.org/10.1016/j.cjche.2016.10.016
1004-9541/

efficiency of these approaches is compared with experimental data and an experimental Pak and Cho equation.

2. Theory

2.1. Tao–Mason equation of state

The common equations of state are based on the van der Waals family of cubic equations, the extended family of virial equations, or equations based more strongly on the results from statistical mechanics and computer simulations [27–29]. The TM EOS belongs to the latter category. Tao and Mason expressed a perturbed correction term that has an effect on the attractive forces, and combined it with the Ihm–Song–Mason (ISM) equation of state [11] to present an advanced equation of state (TM EOS) [12]. This equation of state for pure materials is as follows:

$$\frac{P}{\rho KT}=1+(B_2-\alpha)\rho+\frac{\alpha\rho}{1-\lambda b\rho}+A_1(\alpha-B)b\rho^2\frac{\left(e^{\frac{\kappa T_C}{T}}-A_2\right)}{1+1.8(b\rho)^4} \tag{1}$$

where

$$\begin{aligned}A_1&=0.143\\A_2&=1.64+2.65\left[e^{(K-1.093)}-1\right])\end{aligned} \tag{2}$$

$$\kappa=1.093+0.26\left[(\omega+0.002)^{\frac{1}{2}}+4.50(\omega+0.002)\right] \tag{3}$$

where, ω, λ, ρ, T_c, and KT are the Pitzer acentric factor, an adjustable parameter, number density, critical temperature, and usual meaning. Also, B_2, α and b are the second virial coefficient, the scaling parameter, and the effective van der Waals co-volume.

The TM EOS requires usage of the second virial coefficient (B_2) in company with the parameters α, and b. It should be mentioned that knowledge of experimental second virial coefficient data is adequate to calculate values of the other two temperature-dependent parameters, if the intermolecular potential is not accessible [12]. In this case, there are numerous correlation schemes, typically based on the corresponding state principal that leads to the computation of the second virial coefficient.

Tao and Mason formulated α, and b in terms of the Boyle temperature (T_B) and the Boyle volume (v_B) [12]. However, the B_2 values can be calculated from the Tsonopolous correlation [30] in the absence of sufficient experimental data.

$$B_2\left(\frac{P_C}{RT_C}\right)=f^{(0)}(T_r)+\omega f^{(1)}(T_r) \tag{4}$$

$$f^{(0)}(T_r)=0.1445-\frac{0.330}{T_r}-\frac{0.1385}{T_r^2}-\frac{0.0121}{T_r^3} \tag{5}$$

$$f^{(1)}(T_r)=0.0637+\frac{0.331}{T_r^2}-\frac{0.423}{T_r^3}-\frac{0.008}{T_r^8} \tag{6}$$

In this project, to attain higher accuracy, a corresponding state correlation was examined in order that TM EOS might be applied to nanofluids. In this respect, the following correlation equation for B_2 using a new scaling parameter with minimum input (such as molar density at the room temperature) has been extended. This correlation for second virial coefficient is presented as follows:

$$\begin{aligned}B_2\rho_r=1.033&-3.0069\left(\frac{298.15}{T}\right)-10.588\left(\frac{298.15}{T}\right)^2\\&+13.096\left(\frac{298.15}{T}\right)^3-9.8968\left(\frac{298.15}{T}\right)^4\end{aligned} \tag{7}$$

where ρ_r is density at room temperature.

Tao and Mason's observation shows that the dimensionless quantities α/v_B and b/v_B as almost common functions of the reduced temperature (T/T_B) can be calculated from the exponential formulas based on a LJ (12–6) potential [12]. At this point, the scaling factors (T_B and v_B) are the Boyle temperature and Boyle volume, which can be stated based on the room parameters. The empirical equations given in [12] for α/v_B and b/v_B as, a function of T/T_B can be rescaled by 298.15 K and ρ_r, temperature and density in room point, instead of T_B and v_B as Eslami [31]. Therefore, the input parameter decreased, and this parameter easily obtains in contrast to Boyle parameters or boiling parameters.

$$\alpha\rho_r=a_1e^{-c_1\left(\frac{T}{298.15}\right)}+a_2\left[1-e^{-c_2/\left(\frac{T}{298.15}\right)^{1/4}}\right] \tag{8}$$

$$b\rho_r=a_1\left[1-c_1\left(\frac{T}{298.15}\right)\right]e^{-c_1\left(\frac{T}{298.15}\right)}+a_2\left\{1-\left[1+\frac{c_2}{4\left(\frac{T}{298.15}\right)^{1/4}}\right]e^{\frac{-c_2}{\left(\frac{T}{298.15}\right)^{1/4}}}\right\} \tag{9}$$

where the constants a_1, a_2, c_1, and c_2 are −0.0860, 2.3988, 0.5624, and 1.4267, respectively. In the previous study, TM EOS was extended to the refrigerant mixtures with following equation [19].

$$\frac{P}{\rho KT}=1+\rho\sum\nolimits_{ij}x_ix_j\left((B_2)_{ij}-\alpha_{ij}\right)+\rho\sum_{ij}x_ix_j\alpha_{ij}G_{ij}+\rho\sum_{ij}x_ix_j(I_1)_{ij} \tag{10}$$

The G_{ij} term is the pair distribution function and was calculated by Ihm *et al.* [11]:

$$G_{ij}=\frac{1}{1-\eta}+\left[\frac{b_ib_j}{b_{ij}}\right]^{1/3}\frac{\rho\sum_Kx_Kb_K^{2/3}\left(\lambda_K-\frac{1}{4}\right)}{(1-\eta)(1-\rho\sum_Kx_Kb_K\lambda_K)} \tag{11}$$

where η is the packing fraction of the mixture:

$$\Phi_{mix}=\frac{\rho\sum_Kx_Kb_K}{1+1.8\rho^4\left(\sum_Kx_Kb_K\right)^4} \tag{12}$$

$$\zeta_{mix}=0.143[\exp(K_{mix}T_{cmix}/T-A_{2mix}] \tag{13}$$

that

$$T_{cmix}=\sum\nolimits_Kx_KT_{cK} \tag{14}$$

where T_{cmix} is the traditional pseudocritical temperature.

In the present method, the second virial coefficient and the other two temperature-dependent parameters evaluation can be extended to mixtures using simple geometric mean of liquid density at the room temperature; *i.e.*,

$$\left(\rho_{bp}\right)_{ij}^{-1/3}=1/2\left[\left(\rho_{bp}\right)_i^{-\frac{1}{3}}+\left(\rho_{bp}\right)_j^{-\frac{1}{3}}\right] \tag{15}$$

The adjustable parameter (λ) obtains from volumetric properties at high temperature and pressure and authorizes the whole procedure as self-correcting.

3. ANN Modelling

The artificial neural network (ANN) is the nonlinear mathematical method that attracts the greatest interest due to its simplicity, flexibility, and availability for various training algorithms, as well as its large modelling capacity [32–34]. An artificial neural network, which is derived based on the activity process of the human brain, has hitherto been employed for modelling by many scientific disciplines [33–36]. Several applications and good descriptions of the artificial neural network (ANN) were presented in previous publications [37,38].

The ANN forms the input layer (independent variables), the output layer (dependent variables), and one or more neuron layers called hidden layers can be located between them. The structure of an ANN is described by the number of its layers, the number of neurons in each layer, and the nature of learning algorithms and neurons transfer functions. The important elements of a neural network are the neurons, which are organized in input and output layers of hidden layers (Fig. 1).

3.1. Principal component analysis

Principal component analysis (PCA) is a statistical method that changes an orthogonal transformation, to convert a set of observations of possibly correlated variables into a set of values of linearly uncorrelated variables called principal components. It is a way of recognizing patterns in data, and expressing the data in such a way as to highlight their similarities and dissimilarities. While patterns in data can be hard to find in data of high dimension, the PCA is a great tool for analysing data. The other key benefit of the PCA is that once you have found these patterns in the data, you can compress the data by means of reducing the number of dimensions without much loss of information. Principal components are guaranteed to be independent if the data set is jointly normally distributed. The PCA is sensitive to the relative scaling of the original variables [39].

Finally, the PCA was used to make a classifier system more effective and it is based on the assumption that most information about classes is contained in the directions, including which the variations are the largest. The most common derivation of the PCA is in terms of a standardized linear projection, which maximizes the variance in the projected space [40]. The details of the PCA are stated in [41].

3.2. Network training and selection of the best network architecture

The most regular neural network technique for solving difficulties is multilayer perceptrons (MLP). The MLP discovers the data pattern using algorithms known as "training", these algorithms modify weights of the neurons according to the error between the values of actual output and target output that provide nonlinear regression between inputs and outputs variables and are extremely useful for recognizing patterns in complex data. An example of training algorithms is the back-propagation algorithm that is widely used to train ANN in various applications.

Two transfer functions that are used in the hidden layer and output layer are "Tansig" and "Purelin", respectively. The back propagation algorithm of Levenberg–Marquardt (trainlm) was applied to determine optimal net structure. The trial and error approach is most basic method of training a neural network. The number of hidden layers is to be selected depending on the complexity of the problem but, generally, one hidden layer is satisfactory for modelling most of the problems. In this method, firstly the number of hidden layers considered one and in the next step, in the trial and error approach, the number of neurons in the hidden layer is varied one by one to attain the desired objective function outputs. This trend is continued to find the number of neurons that leads to the lowest error for the testing subset and is reported as the optimum number of neurons in the hidden layer.

The mathematical definition of the error criteria, including average deviation percentage (AAD) and correlation coefficient (R^2) values, were given as below:

$$\mathrm{AAD} = \frac{1}{N}\sum_{i=1}^{N}\left(\left|\frac{\rho_i^{\mathrm{exp}} - \rho_i^{\mathrm{cal}}}{\rho_i^{\mathrm{exp}}}\right|\right) \times 100\% \tag{16}$$

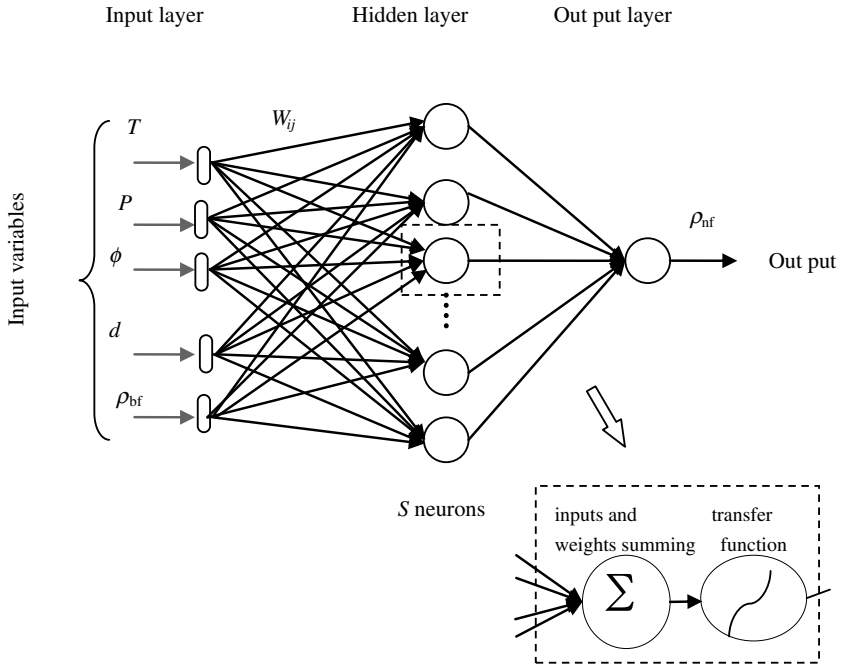

Fig. 1. The topology of a three layer MLP.

$$R^2 = \frac{\sum_{i=1}^{N}\left(\rho_i^{exp}-\bar{\rho}\right)^2-\sum_{i=1}^{N}\left(\rho_i^{exp}-\bar{\rho}_i^{cal}\right)^2}{\sum_{i=1}^{N}\left(\rho_i^{exp}-\bar{\rho}\right)^2} \quad (17)$$

4. Results and Discussion

In this project, the density, specific heat capacity, and isentropic compressibility (K_s) of some nanofluids such as Sb_2O_5, SnO_2/(EG + H_2O), ZnO/(EG + H_2O), Al_2O_3/(EG + H_2O), ZnO/(PEG + H_2O), ZnO/PEG, and TiO_2/EG were estimated from the extended TM EOS at various temperatures and volume fractions. In addition, the artificial neural network with PCA technique has been utilized to compute the densities of the aforementioned nanofluids as a function of the temperature, volume fraction of nanoparticle, diameter of nanoparticle, and the densities of base fluids and ranges of input–output variables for each nanofluid are given in Table 1.

Table 1
Summary of the input–output dataset characterization

Nanofluids	Temperature/K	Volume fraction	Density base fluids/mol·L^{-1}	Density nanofluids/ mol·L^{-1}
ZnO/(EG + H_2O)	273.15–323.15	0.0006–0.004	23.66–25.51	24.57–25.88
Al_2O_3/(EG + H_2O)	273.15–323.15	0.0008–0.006	23.73–24.99	23.87–24.69
Sb_2O_5,SnO_2/(EG + H_2O)	273.15–323.15	0.0035–0.0180	25.25–29.88	25.20–29.45
ZnO/PEG	293.15–318.15	0.001–0.340	18.45–18.80	18.44–18.52
ZnO/(PEG + H_2O)	293.15–318.15	0.001–0.354	14.28–26.34	14.25–26.11
TiO_2/EG	283.15–343.15	0.0031–0.0088	17.22–18.39	17.56–18.96

Experimental densities for Sb_2O_5, SnO_2/(EG + H_2O), ZnO/(EG + H_2O), and Al_2O_3/(EG + H_2O)were obtained from Vajjha and Mahagaonkar [42]. Furthermore, the experimental densities for ZnO/(PEG + H_2O) and ZnO/PEG were attained from [43] and the experimental densities for TiO_2/EG were determined from [44].

The equation for the density of two-phase mixtures for particles of micrometre size is available in the literature on slurry flows [45]. Pak and Cho [46] adopted the same equation for nanometre sized particles, which is expressed by the formula

$$\rho_{nf} = \rho_p\varphi + \rho_{bf}(1-\varphi) \quad (18)$$

where n_g is the density of the nanofluid, ρ_p is the density of the particle, φ is the particle volume concentration, and ρ_{bf} is the density of the base fluid. Pak and Cho conducted the experiment at only one temperature (298 K) for γ-Al_2O_3 and TiO_2nanofluids up to 4.5% volume concentration to verify Eq. (4).

As above mentioned, the experimental evaluation of nanofluids have many limitations, such as complexities in preparing mono-disperse suspensions, methodological problems in measuring particle size, concentration, and the homogeneity of its solution. Hence, several density measurements have been presented for various nanofluids in different situations [10]. Therefore, novel approaches such as equation of state and artificial neural networks are efficient in predicting the density and other thermodynamic properties of nanofluids, based on available data.

In this investigation, the TM equation of state was used to determine the density of base fluids. Then we replaced the density of the base fluid in the Pak and Cho [46] equation and introduced a new equation of state to determine the density of nanofluids for the first time.

Extension of statistical, mechanically-based equation of state for pure and mixed liquids requires preliminary modifications of the TM EOS. In the beginning, the second virial coefficient was developed using the density of liquid at room temperature that can simply be measured in contrast to the critical parameters. Consequently, the number of input parameters in the Tsonopolous'correlation [30] (critical temperature, critical pressure, and acetric factor) are reduced to one parameter, including density at room temperature (ρ_r).

Besides, kin Eq. (2) is a weak function of the acentric factor so that *k*is approximated to 1.093 and A_2 was estimated to 1.64 [47]. Then, the parameters α and b were correlated by means of Eqs. (8) and (9), respectively. In both equations, the input parameters (the molar density at room temperature) are more available than the Boyle temperature and volume, and these modifications lead to a decrease in the number of input parameters of B_2, α and b from five (including critical temperature, critical pressure, acentric factor, Boyle temperature, and Boyle volume) to one (molar density at room temperature).

In addition, the parameter of λ for pure base fluid was adjusted by the nonlinear regression method as follow:

$$\lambda = a + bT + cT^2 + dT^3 \quad (19)$$

where the parameters that were used for calculation of λ are listed in Table 2. After that, with these modifications using Pak and Cho's [46] equation, the densities of nanofluids can be computed.

Table 2
Coefficients in Eq. (19)

Nanofluids	a	b	$c \times 10^{-3}$	$d \times 10^{-6}$
EG	1.9918	−0.0165	0.05643	0.0639-
PEG	0.5363	−0.0003	0.0292	4.9939
H_2O	0.8615	−0.0033	0.0097	−0.0102

The MLP is trained, validated, and tested at random with 70% (199 data points), 15% (43 data points), and 15% (43 data points), respectively.

At first, a set of observations are converted into a set of values of linearly uncorrelated variables with a statistical method: namely, principal component analysis (PCA). The number of principal components variable in this work is equal to the number of original variables but the variables values of linearly uncorrelated.

In the second step of the training procedure, all data points produced from PCA were scaled to the range of [0, 1] as follows:

$$\text{Output} = \frac{\text{input}-\min(\text{input})}{\max(\text{input})-\min(\text{input})} \times 1 + 0 \quad (20)$$

The possibility of over-training is a problem in the ANN, and can be overcome by suitable selection of the number of neurons in the hidden layer. The numbers of hidden neurons were determined by trial and error and were begun with two neurons in the hidden layer, with the

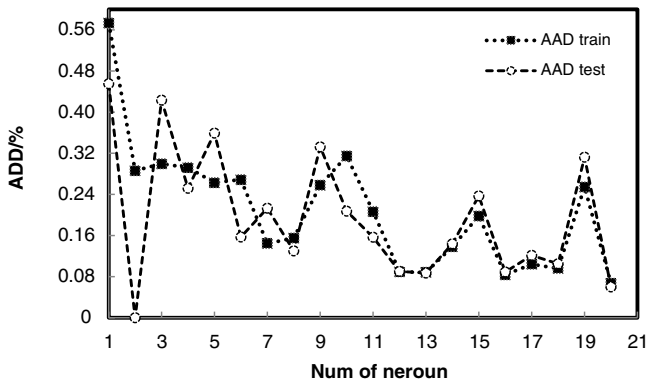

Fig. 2. Effect of the number of hidden layer neurons on AAD.

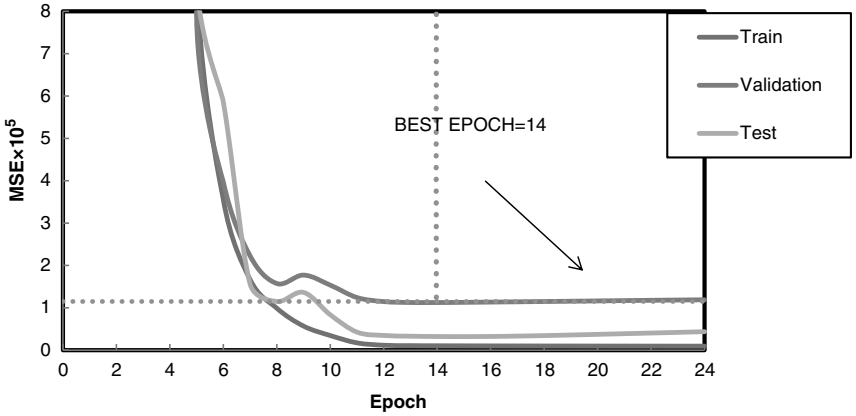

Fig. 3. Evolution of training, validation, and test errors as a function of the number of training epochs during ANN training.

number of neurons increased regularly. The performance of the network in training phase should increase with the increase in the number of neurons; at the same time as the performance of the network in testing data phase leads to the optimum value of hidden neurons (see Fig. 2). In this project, the mean square error (MSE) was chosen as a compute of the performance of the neural network. The net with one hidden layer (20 neurons) and with a mean square error of 1.12×10^{-5} leads to the most excellent prediction in Fig. 2. Fig. 3 shows the progress of training, validation, and test errors as a function of the number of training epochs (based on an early stopping approach).

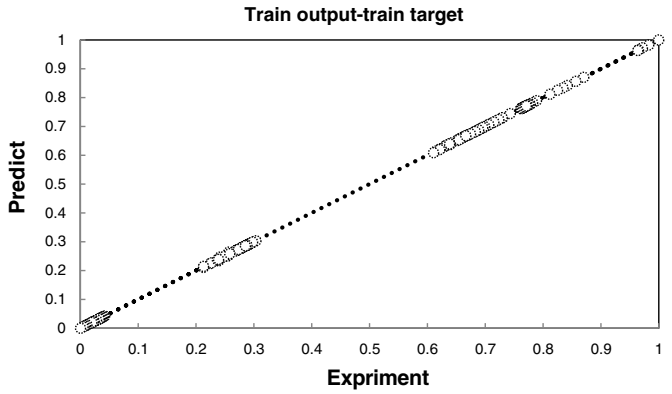

Fig. 4. Modelling ability of the optimized ANN to predict the effective densities of all nanofluids suspension: ($R^2 = 0.999$, AAD = 0.48%).

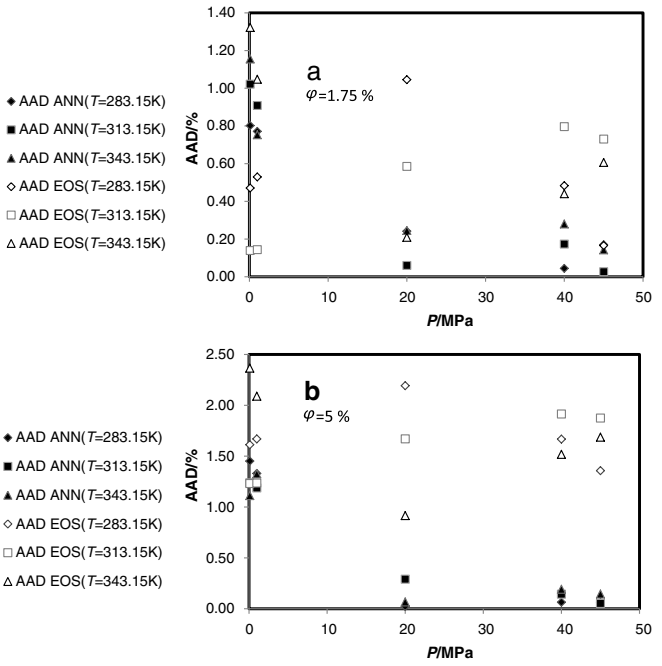

Fig. 6. Deviation plot for the calculated density of TiO_2/EG from TM EOS and ANN at different temperatures, pressures and two volume fractions (Fig. 6a. ($\phi = 1.75\%$) and (Fig. 6b). $\phi = 5\%$), compared with the experiment [44].

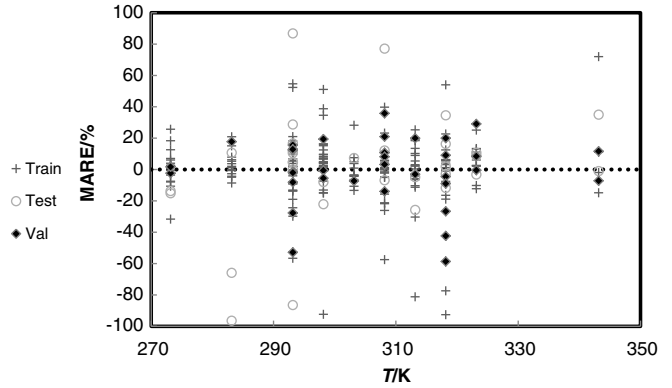

Fig. 5. Mean absolute relative error for the train, test and validation of densities of all nanofluids with the experimental data.

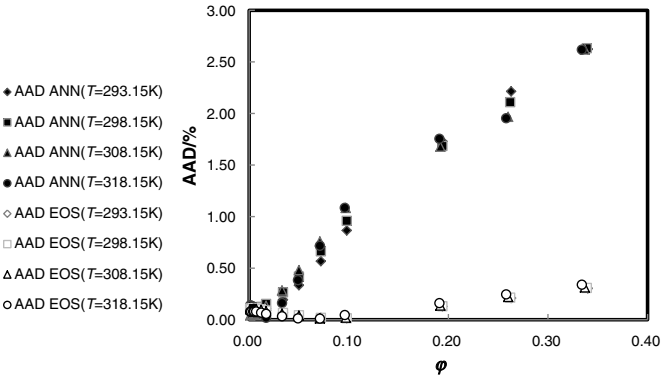

Fig. 7. Deviation plot for the calculated density of ZnO/PEG from TM EOS and ANN at different temperatures and volume fractions, compared with the experiment [43].

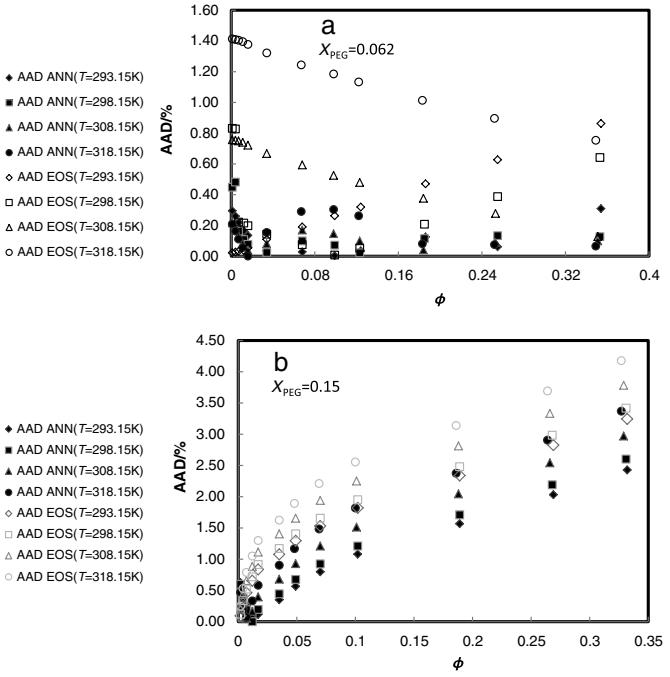

Fig. 8. Deviation plot for the calculated density of ZnO/PEG + H_2O from TM EOS and ANN at different temperatures, volume fractions and two mole fraction of PEG (a: $X_{PEG} = 0.062$ and b: $X_{PEG} = 0.15$) compared with the experiment [43].

Based on testing data, the optimized neural network model was used to predict the densities of nanofluids; the evaluation between predictive values and experimental values is carried out and shown in Fig. 4. The results of Fig. 4 demonstrate good agreement between the predicted and the experimental values of densities of mentioned nanofluids with an absolute average error, AAD% = 0.48%, and high correlation coefficients, $R^2 = 0.999$.

The error analysis of trained net over temperature variation for train, test, and validation point are presented in Fig. 5.

TM EOS was combined with Pak and Cho's equation to calculate densities of TiO_2/EG nanofluids and compare with experimental data [44] at different temperatures, pressures, and two volume fractions (1.75% and 5%) (Fig. 6). The results show that these models have a good level of agreement with experimental data [45]. The AAD of densities of TiO_2/EG from new EOS and the ANN with experimental data at volume fraction 1.75% are 0.58% and 0.48%, respectively. In addition, the AAD at volume fraction 5% are 1.67% and 0.58%, respectively. Fig. 7 shows the deviation plot for the calculated density of ZnO/PEG from new EOS and ANN at different temperatures and volume fractions compared with the experiment [43], and the AAD of these models from the literature are 0.67% and 0.11%.

The deviation plot for the calculated density of ZnO/PEG + H_2O from TM EOS and ANN at different temperatures, volume fractions, and two mole fractions of PEG (0.062 and 0.15) compared with the experiment [43]. The absolute average deviations of these models from experimental data at mole fraction of 0.062 are 0.59% and 0.14%, respectively (see Fig. 8a). Also, the AAD at mole fraction of 0.15 are 1.62% and 1.05%, respectively (see Fig. 8b).

The absolute average deviation from experimental data [42] for the predicted densities of the three systems (Al_2O_3/(EG + H_2O), Sb_2O_5, SnO_2/(EG + H_2O); and ZnO/(EG + H_2O)) are calculated from new EOS, ANN, and experimental Pak and Cho, and are presented in Figs. 9–11.

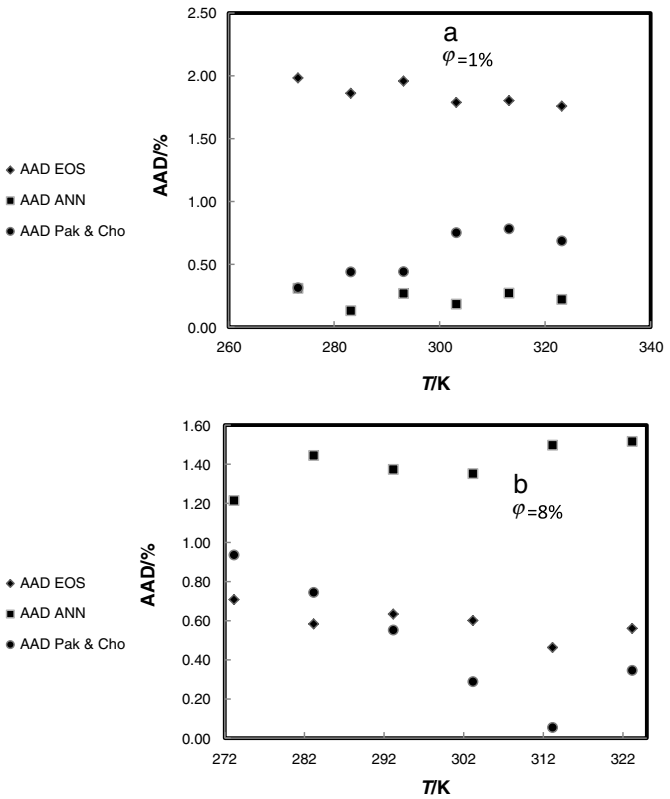

Fig. 9. Deviation plot for the calculated density of Al_2O_3/(EG + H_2O) from TM EOS, ANN and Pak & Cho at different temperatures and two volume fractions (a: $\phi = 1\%$ and b: $\phi = 8\%$), compared with the experiment [42].

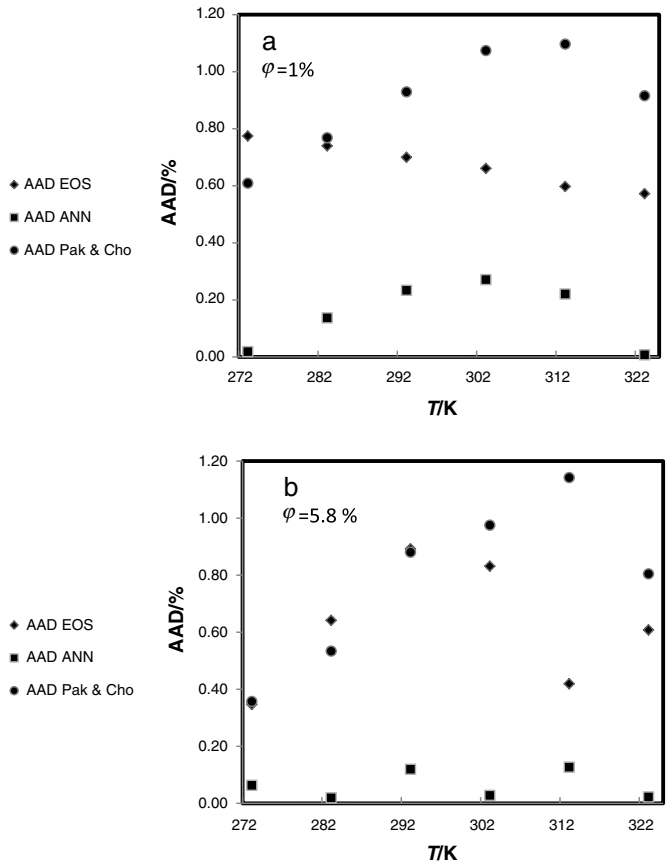

Fig. 10. Deviation plot for the calculated density of Sb_2O_5, SnO_2/(EG + H_2O) from TM EOS, ANN and Pak & Cho at different temperatures and two volume fractions (a: $\phi = 1\%$ and b: $\phi = 5.8\%$), compared with the experiment [42].

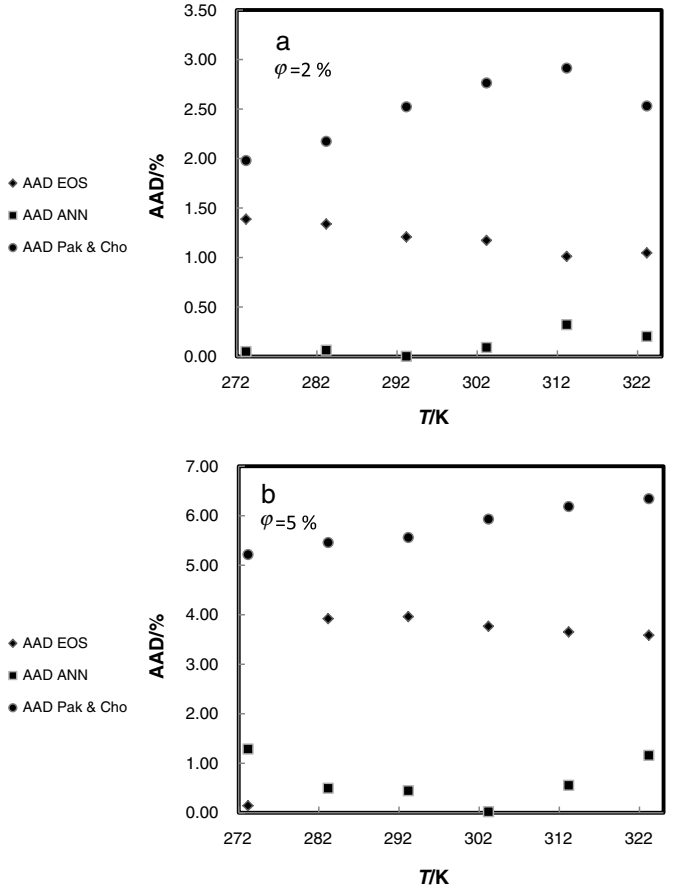

Fig. 11. Deviation plot for the calculated density of ZnO/(EG + H_2O) from TM EOS, ANN and Pak & Cho at different temperatures and two volume fractions (a: $\phi = 2\%$ and b: $\phi = 5\%$), compared with the experiment [42].

It should be stated that in the experimental Pak and Cho, densities of base fluids are obtained from experimental data, while in the first model the densities of base fluids are computed from TM EOS. These figures show that the ANN model is in good agreement with experimental data and is superior to others. Also, the new EOS is better than the experimental Pak and Cho.

In this research, some thermodynamic properties such as heat capacity and isentropic compressibility of nanofluids can are predicted using the equations below:

$$C_{p(\mathrm{nf})} = \frac{\varphi_{(\mathrm{np})} \times C_{p(\mathrm{np})} + (1-\varphi)\rho_{(\mathrm{bf})} \times C_{p(\mathrm{bf})}}{\rho_{(\mathrm{nf})}} \quad (21)$$

$$k_s = \frac{1}{du^2} \quad (22)$$

where d and u are density and speed of sound of nanofluids, respectively.

The deviation plot for the calculated heat capacity of ZnO/PEG at different temperatures and volume fractions is compared with the experiment [43] in Fig. 12. It can be seen from this figure that the calculated heat capacity has good agreement with literature with AAD = 1.04%.

In addition, the plot of deviation of heat capacity of ZnO/(PEG + H_2O) at different temperatures, volume fractions, and mole fraction of PEG (0.06 and 0.15) is presented in Fig. 13, and the absolute average deviations for these systems are 1.07% and 0.23%, respectively.

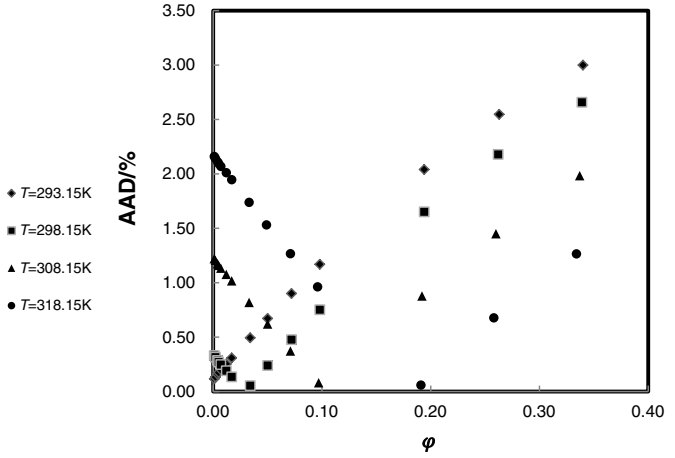

Fig. 12. Deviation plot for the calculated heat capacity of ZnO/PEG from TM EOS at different temperatures and volume fractions, compared with the experiment [43].

As a final point, the calculated isentropic compressibility of ZnO/PEG from Eq. (22) at different temperatures and volume fractions, is compared with the experiment [43] and presented in Fig. 14. The AAD of this system is 0.65%.

The calculated isentropic compressibility of ZnO/PEG + H_2O at different temperatures, volume fractions, and mole fraction of PEG (0.06 and 0.15) is also compared with the literature [43] (see Fig. 15) and the AADs are 0.70% and 0.93%, respectively. Since the values of AAD can establish the fact that the calculated values are more or less close to the experimental data, it can be claimed that the new EOS can predict the experimental density and thermodynamic properties of nanofluids with a high degree of accuracy.

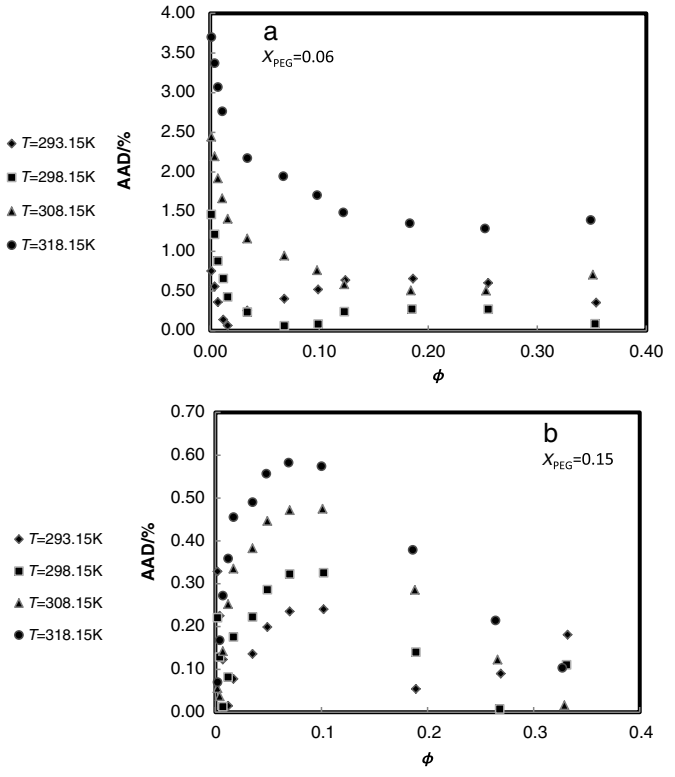

Fig. 13. Deviation plot for the calculated heat capacity of ZnO/(PEG + H_2O) from TM EOS at different temperatures, volume fractions and two mole fraction of PEG (a: $X_{PEG} = 0.06$ and b: $X_{PEG} = 0.15$), compared with the experiment [43].

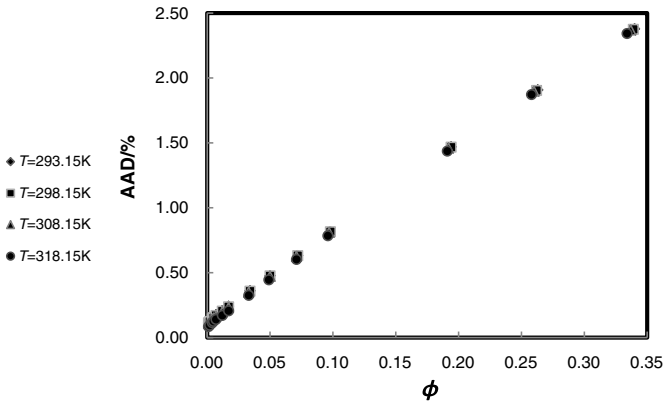

Fig. 14. AAD plot of the calculated isentropic compressibility of ZnO/PEG from TM EOS at different temperatures and volume fractions, compared with the experiment [43].

Table 3 contains the AAD of the calculated molar density of all nanofluids using the EOS and ANN at various temperatures, pressures, and volume fractions. As is clear from Table 3, in most cases the accuracy of the calculated densities using the ANN are superior to new EOS but also that both of them are in agreement with experimental data. The AADs of new EOS and ANN are 1.11% and 0.48%, respectively.

5. Conclusions

In this work, the density, specific heat capacity, and isentropic compressibility (K_s) of some nanofluids such as Sb_2O_5,SnO_2/(EG + H_2O), ZnO/(EG + H_2O), Al_2O_3/(EG + H_2O), ZnO/(PEG + H_2O), ZnO/PEG, and TiO_2/EG were estimated from the extended TM EOS together with the Pak and Cho equation at various temperatures, pressures, and volume fractions. The TM EOS was performed using minimum input (density of room temperature). Also, the artificial neural network + PCA technique (with 20 neuron in hidden layer) was performed over the whole range of available conditions. The AADs of the calculated molar density of all nanofluids using the new EOS and ANN at various temperature, pressure, and volume fractions are 1.11% and 0.48%, respectively. In addition, the heat capacity and isentropic compressibility of the aforementioned nanofluids were predicted using obtained densities of new EOS. The results showed that these properties are in agreement with the literature.

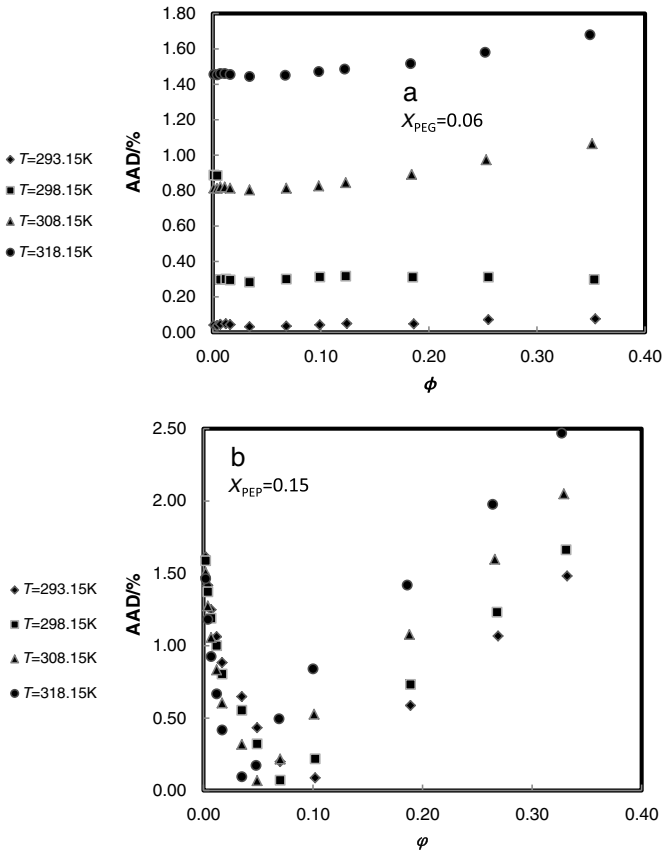

Fig. 15. AAD plot of the calculated isentropic compressibility of ZnO/(PEG + H_2O) from TM EOS at different temperatures, volume fractions and two mole fraction of PEG (a: X_{PEG} = 0.06 and b: X_{PEG} = 0.15), compared with the experiment [43].

Table 3
Result of density prediction for all mentioned nanofluids

Nanofluids	NP	ΔT/K	ΔP×10/MPa	AAD (EOS)/%	AAD (ANN)/%
ZnO/(EG + H_2O)	6	273.15–323.15	1	1.31	0.71
	6	273.15–323.15	1	1.19	0.12
	6	273.15–323.15	1	0.78	0.14
	6	273.15–323.15	1	0.97	0.63
	6	273.15–323.15	1	3.17	0.66
	6	273.15–323.15	1	0.50	0.59
Al_2O_3/(H_2O + EG)	6	273.15–323.15	1	1.86	0.23
	6	273.15–323.15	1	1.49	0.24
	6	273.15–323.15	1	1.08	1.08
	6	273.15–323.15	1	1.60	0.22
	6	273.15–323.15	1	0.59	1.40
	6	273.15–323.15	1	3.05	1.12
Sb_2O_5/(EG + H_2O)	6	273.15–323.15	1	0.67	0.15
	6	273.15–323.15	1	0.11	0.09
	6	273.15–323.15	1	0.34	0.17
	6	273.15–323.15	1	0.45	0.12
	6	273.15–323.15	1	0.62	0.06
ZnO/PEG	56	293.15–318.15	1	0.11	0.67
ZnO/(PEG + H_2O)	48	293.15–318.15	1	1.62	1.05
	48	293.15–318.15	1	0.59	0.14
TiO_2/EG	15	283.15–343.15	1–450	0.58	0.45
	15	283.15–343.15	1–450	1.67	0.58
Overall	284	273.15–343.15	1–450	1.11	0.48

References

[1] P.D. Shima, J. Philip, B.J. Raj, Synthesis of aqueous and nonaqueous iron oxide nanofluids and study of temperature dependence on thermal conductivity and viscosity, *J. Phys. Chem. C* 114 (2010) 18825–18833.
[2] S.U.S. Choi, Development and application of non-Newtonian flows, *ASME* 66 (1995) 99–106 (New York).
[3] W. Xiang-Qi, S.M. Arun, A review on nanofluids - Part I: Theoretical and numerical investigations, *Braz. J. Chem. Eng.* 25 (2008) 613–630.
[4] Y. Ren, H. Xie, A. Cai, Effective thermal conductivity of nanofluids containing spherical nanoparticles, *Appl. Phys.* 38 (2005) 3958–3961.
[5] H.A. Mintsa, G. Roy, C.T. Nguyen, D. Doucet, New temperature dependent thermal conductivity data for water-based nanofluids, *Int. J. Therm. Sci.* 48 (2009) 363–371.
[6] M. Chandrasekar, S. Suresh, B.A. Chandra, Experimental investigations and theoretical determination of thermal conductivity and viscosity of Al_2O_3/water nanofluidExp, *Exp. Thermal Fluid Sci.* 34 (2010) 210–216.
[7] M.M. Papari, F. Yousefi, J. Moghadasi, H. Karimi, A. Campo, Modeling thermal conductivity augmentation of nanofluids using diffusion neural networks, *Int. J. Therm. Sci.* 50 (2011) 44–52.
[8] H. Karimi, F. Yousefi, M.R. Rahimi, Correlation of viscosity in nanofluids using genetic algorithm-neural network (GA-NN), *Heat Mass Transf.* 47 (2011) 1417–1425.
[9] S.E.B. Maïga, S.J. Palm, C.T. Nguyen, G. Roy, N. Galanis, Heat transfer enhancement by using nanofluids in forced convection flows, *Int. J. Heat Fluid Flow* 26 (2005) 530–546.
[10] M.J. Pastoriza-Gallego, C. Casanova, J.L. Legido, M.M. Piñeiro, CuO in water nanofluid: Influence of particle size and polydispersity on volumetric behaviour and viscosity, *Fluid Phase Equilib.* 300 (2011) 188–196.
[11] G. Ihm, Y. Song, E.A. Mason, Strong principle of corresponding states: reduction of a *p-v-T* surface to a line, *Fluid Phase Equilib.* 75 (1992) 117–125.
[12] F.M. Tao, E.A. Mason, Statistical-mechanical equation of state for nonpolar fluids: Prediction of phase boundaries, *J. Chem. Phys.* 100 (1994) 9075–9084.
[13] F. Yousefi, H. Karimi, M. Gomar, Ability of analytical and artificial approaches for prediction of the volumetric properties of some polymer blends, *Fluid Phase Equilib.* 355 (2013) 92–98.
[14] F. Yousefi, H. Karimi, M. Gomar, Volumetric properties of polymer blends from Tao–Mason equation of state, *Polym. Bull.* 70 (2013) 1445–1455.
[15] F. Yousefi, Correlation of volumetric properties of binary mixtures of some ionic liquids with alcohols using equation of state, *Ionics* 18 (2012) 769–775.

[16] F. Yousefi, H. Karimi, M.M. Papari, Extension of Tao–Mason equation of state to heavy n-alkanes, *Chin. J. Chem. Eng.* 21 (2013) 894–900.
[17] F. Yousefi, Modeling the volumetric properties of polymer melts using equation of state, *High Temp. High Press.* 42 (2013) 211–226.
[18] F. Yousefi, H. Karimi, R. Ghafarian Shirazi, M. Gomar, Prediction of PVT properties of pure and mixture of polymer melts using modified Ihm-song-Mason equation of state, *High Temp. High Press.* 42 (2013) 451–467.
[19] F. Yousefi, H. Karimi, Application of equation of state and artificial neural network to prediction of volumetric properties of polymer melts, *J. Ind. Eng. Chem.* 19 (2013) 498–507.
[20] F. Yousefi, H. Karimi, P-V–T properties of polymer melts based on equation of state and neural network, *Eur. Polym. J.* 48 (2012) 1135–1143.
[21] F. Yousefi, H. Karimi, Z. Gandomkar, Equation of state and artificial neural network to predict the thermodynamic properties of pure and mixture of liquid alkali metals, *Fluid Phase Equilib.* 370 (2014) 43–49.
[22] Z. Zhang, K. Fried, Artificial neural networks applied to polymer composites: a review, *Compos. Sci. Technol.* 63 (2003) 2029–2036.
[23] A. Khajeh, H. Modarress, Application of adaptive Neuro fuzzy inference system for solubility prediction of carbon dioxide in polymers, *Expert Syst. Appl.* 37 (2010) 3070–3074.
[24] F. Gharagheizi, G.R. Salehib, Prediction of enthalpy of fusion of pure compounds using an artificial neural network-group contribution method, *Thermochim. Acta* 521 (2011) 37–40.
[25] A. Sencan, I. IlkeKöse, R. Selbas, Prediction of thermophysical properties of mixed refrigerants using artificial neural network, *Energy Convers. Manag.* 52 (2011) 958–974.
[26] A. Ghaedi, Simultaneous prediction of the thermodynamic properties of aqueous solution of ethylene glycol monoethyl ether using artificial neural network, *J. Mol. Liq.* 207 (2015) 327–333.
[27] J.M.H. Levelt Sengers, U.K. Deiters, U. Klask, P. Swidersky, G.M. Schneider, Application of the Taylor dispersion method in supercritical fluids, *Int. J. Thermophys.* 14 (1993) 893–922.
[28] S.I. Sandler, Chemical and Engineering Thermophysics, Wiley, New York, 1989.
[29] J.M. Prauznitz, R.N. Lichtentaler, E.G. Azevedo, Molecular Thermodynamics of Fluid Phase Equilibria, Prentice-Hall, Englewood Cliffs, NJ, 1999.
[30] C. Tsonopolous, Second virial coefficients of water pollutants, *AICHE J.* 24 (1978) 1112–1127.
[31] H. Eslami, Equation of state for nonpolar fluids: prediction from boiling point constant, *Int. J. Thermophys.* 21 (2000) 1123–1136.
[32] S. Haykin, Neural Networks: A Comprehensive Foundation, second ed. Prentice-Hall, New York, 1999.
[33] P. Xu, S. Xu, H. Yin, Application of self-organizing competitive neural network in fault diagnosis of suck rod pumping system, *J. Pet. Sci. Eng.* 58 (2007) 43–48.
[34] B. Vaferi, Y. Rahnam, P. Darvishi, A.R. Toorani, M. Lashkarbolooki, Phase equilibria estimation of binary systems containing ethanol using optimal feedforward neural network, *J. Supercrit. Fluids* 84 (2013) 80–88.
[35] B. Vaferi, M. Karimi, M. Azizi, H. Esmaeili, Comparison between the artificial neural network, SAFT and PRSV approach in obtaining the solubility of solid aromatic com- pounds in supercritical carbon dioxide, *J. Supercrit. Fluids* 77 (2013) 45–51.
[36] B. Vafaei, R. Eslamloueyan, S. Ayatollahi, Simulation of steam distillation process using neural networks, *Chem. Eng. Res. Des.* 87 (2009) 997–1002.
[37] C. Bishop, Neural Networks for Pattern Recognition, Oxford Clarendon, Oxford, 1996.
[38] B. Ripley, Pattern Recognition and Neural Networks, Cambridge University Press, Cambridge, 1996.
[39] K. Pearson, On lines and planes of closest fit to systems of points in space, *Philosophical Magazine* 2 (1901) 559–572, doi:10.1080/14786440109462720.
[40] X. Wang, K.K. Paliwal, Feature extraction and dimensionality reduction algorithms and their applications in vowel recognition, *J. Pattern Recognit. Soc.* 36 (2003) 2429–2439.
[41] Lindsa IS, A tutorial on principal components analysis, http://kybele.psych.cornell.edu/~edelman/Psych-465 (Spring-2003/PCA- tutorial) (2002).
[42] R.S. Vajjha, D.K. Das, B.M. Mahagaonkar, Density measurement of different nanofluids and their comparison with theory, *Pet. Sci. Technol.* 27 (2009) 612–624.
[43] M.T. Zaafarani-Moattar, R. Majdan-Cegincara, Effect of temperature on volumetric and transport properties of nanofluids containing ZnO nanoparticles poly(ethylene glycol) and water, *J. Chem. Thermodyn.* 54 (2012) 55–67.
[44] D. Cabaleiro, M.J. Pastoriza-Gallego, C. Gracia-Fernandez, M.M. Pineiro, L. Lugo, Rheological and volumetric properties of TiO_2-ethylene glycol nanofluids, *Nanoscale Res. Lett.* 8 (2013) 286–298.
[45] N.P. Cheremisinoff, Encyclopedia of Fluid Mechanics, Slurry Flow Technology, vol. 5, Gulf Publishing, Houston, TX, 1986.
[46] B.C. Pak, Y.I. Cho, Hytiodynamic and heat transfer study of dispersed fluids with submicron metallic oxide particles, *Exp. Heat Transfer* 11 (1998) 151–170.
[47] M.M. Papari, M. Kiani, R. Behjatmanesh-Ardakani, J. Moghadasi, A. Campo, Equation of state and *P–V–T* properties of polymer melts based on glass transition data, *J. Mol. Liq.* 161 (2011) 148–152.